ELSEVIER

Journal of Hydrology 268 (2002) 143–157

Journal of Hydrology

www.elsevier.com/locate/jhydrol

A comparison of published experimental data with a coupled lattice Boltzmann-analytic advection–diffusion method for reactive transport in porous media

G.S. O'Brien*, C.J. Bean, F. McDermott

Department of Geology, University College Dublin, Belfield, Dublin, Ireland

Received 16 July 2001; revised 18 June 2002; accepted 24 June 2002

Abstract

Many processes in the Earth's crust are controlled by the chemical and physical interactions between fluids and geological media where the lattice is usually characterised by a heterogeneous permeability, intrinsic rock permeability and fault networks. Dissolution/precipitation of rock minerals and chemical transport can alter the rock properties, which leads to a change in the flow characteristics and alteration of the geological media with time. In this article, we propose a novel method for modelling heterogeneous reactive transport with a feedback between the flow and chemical alterations. To model fluid flow, we use a modified lattice Boltzmann scheme which facilitates the incorporation of complex boundary conditions and enables us to examine flow in heterogeneous media. In addition, the local update rules of this scheme allow the code to be parallelised on multiple processors. We have coupled transport of chemical species and reactive flow to this scheme using a solution to the advection–diffusion equation. Experimentally derived dissolution/precipitation rates are used to calculate rates of interaction between minerals and the fluids with which they are in contact. Laboratory scale passive and reactive flow-cell experiments from the literature have been used to test and validate the accuracy of the transport of the chemical species in a heterogeneous porous medium. We have also examined the output of our scheme for water–rock interactions in a quartzofeldspathic lithology for relatively long periods of geological time. We have focused on quartz and feldspar reactive flow with associated secondary clay minerals, as these are some of the most abundant minerals in the Earth's crust. In all cases, the numerical results agree well with the experimental results from our numerical scheme. The scheme also reproduces alteration of a quartzofeldspathic lithology over geological time periods, consistent with other numerical work.

Keywords: Flow modelling; Chemical feedbacks; Dissolution rates; Heterogeneity; Lattice Boltzmann; Fluid–rock interactions

1. Introduction

Fluid–rock interactions control a wide variety of processes in Earth Sciences including hydrocarbon migration, mineralisation, groundwater evolution and diagenesis. These processes involve dissolution, precipitation and chemical species transport which alter the rock matrix and lead to feedbacks between the flow characteristics and geological media. A detailed review of reactive flow is beyond the scope of this paper but a broad outline of the theory is given by

* Corresponding author.
E-mail addresses: gareth.obrien@ucd.ie (G.S. O'Brien), chris.bean@ucd.ie (C.J. Bean), frank.mcdermott@ucd.ie (F. McDermott).

0022-1694/02/$ - see front matter
PII: S0022-1694(02)00173-7

Phillips (1991). Reactive transport schemes can provide useful insights into many processes, but the development of realistic models remains complex. Challenges in modelling flow and reactions in porous media include the incorporation of heterogeneity, chemical kinetics and the simulation of large-scale multi-component models. Physical and chemical heterogeneities play a crucial role in determining the evolution of the system. Fluid flow in the Earth's crust is controlled by fracture networks and intrinsic rock permeability, and there is abundant evidence that fault networks and rock permeability obey fractal statistics (Korvin, 1992; Bonnet et al., 2001). While the permeability of such systems may be approximated, a more accurate solution could be found from models, which replicate the transport of fluids through such heterogeneous media. One over-simplification, which is often employed, for example, is that equilibrium thermodynamics is the usual basis for calculating chemical interactions whilst kinetic effects are often neglected. The incorporation of kinetics into models provides a more complete behaviour of the temporal evolution of fluid/rock systems. Most current schemes use a continuum approach to model reactive transport as summarised recently (Lichtner et al., 1996). Early work was computationally restricted but recent advances have enabled the simulation of large-scale, multi-component models. Improved chemical kinetic data from controlled laboratory experiments have enabled recent models to incorporate realistic mineral reaction rates (Canals and Meunier, 1995). Also, progress has been made on the simulation of heterogeneity in geological media (Bolton et al., 1997, 1999). However, with most finite difference methods, where continuum differential equations are numerically solved using a finite difference scheme, the inclusion of heterogeneity must be treated cautiously. This paper outlines our approach to model reactive transport and validates the scheme against laboratory results for passive and reactive transport. The approach used is a discrete scheme for modelling fluid flow, which we have modified to include reactive transport. We have adopted this approach as heterogeneity is intrinsic to the scheme, chemical kinetics are easily included and the method can be easily parallelised to run on multiple processors. We have focused on a two dimensional model to verify the applicability of our method, but the scheme can easily be extended to three dimensions. The lattice Bhatnagar–Gross–Krook (BGK) method used to model flow is discussed in Section 2. Section 3 details the transport of solutes through porous media and validates the scheme against passive transport of a tracer through a porous medium. The incorporation of reactive flow and the comparison of our scheme against flow-through dissolution experiments are considered in Section 4. Finally, in Section 5, the alteration of a quartz–feldspar rock is outlined to explore the output of our scheme for geological timescales and geochemically realistic alteration processes.

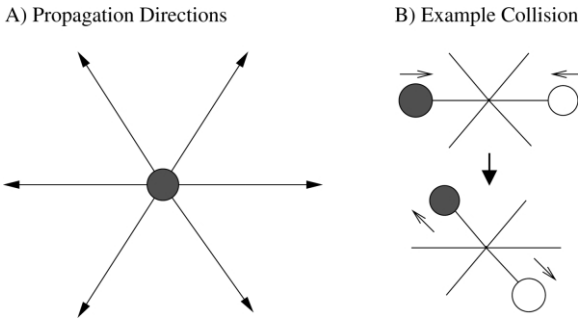

Fig. 1. The update rules for the 2D lattice gas model. The particles have unit mass and velocity and propagate to the nearest neighbours (A). An example collision with two particles is shown in (B). The top refers to the state before the collision and the bottom to the state after the collision.

2. Lattice Bhatnagar–Gross–Krook method

Fluid flow in porous media is modelled using a modified version of the lattice BGK technique. This technique has evolved from the lattice gas automata (LGA) (Frisch et al., 1986). The LGA scheme is a cellular automaton model for the solution of the Navier–Stokes equation for fluid flow. In the LGA scheme, a system of identical fluid particles is confined to a hexagonal lattice. The particles rest either on the nodes or move along the six connecting directions at unit vector $\mathbf{e}_i$ where the subscript i denotes the direction (Fig. 1(A)). An exclusion principle holds on each node, as only one particle is allowed to reside there. If two or more particles arrive at the same node they interact through collisions, which conserve momentum and density (Fig. 1(B)).

The density ρ and momentum $\rho\mathbf{u}$ at each node are given by:

$$\rho = \sum_{i=0}^{6} N_i(\mathbf{x}, t) \tag{1}$$

$$\rho\mathbf{u} = \sum_{i=0}^{6} N_i(\mathbf{x}, t)\mathbf{e}_i \tag{2}$$

$N_i(\mathbf{x}, t)$ is a Boolean variable indicating the presence or absence of a particle at a node $\mathbf{x}$ at time t propagating on the lattice in direction i. The node points are defined as solid if particles cannot propagate through. In this case, particles are reflected 180°, otherwise the node points are void sites (100% porous). This discrete nature of the node points allows the simulation of fluid flow in complex geometries to be easily implemented.

However, the Boolean nature of the fluid particles, the presence or absence of a particle at a node, requires large temporal and spatial averaging. To overcome this the lattice Boltzmann (LB) method was introduced (McNamara and Zanetti, 1988). The Boolean variable $N_i(\mathbf{x}, t)$ was replaced with a probability of a particle residing at node $\mathbf{x}$, at time t, propagating in direction i. In the BGK scheme (Qian et al., 1992), the collision step of the LB method is replaced by relaxation to an equilibrium distribution. This reduces the collision step to multiplication by a single relaxation parameter. With properly chosen equilibrium distributions, the Navier–Stokes equation is obtained. The fluid probability density $N_i(\mathbf{x}, t + \Delta t)$ moving in direction i at node $\mathbf{x}$ from node $\mathbf{x} - \mathbf{e}_i$ at time $t + \Delta t$ is given by

$$N_i(\mathbf{x}, t + \Delta t) = N_i(\mathbf{x} - \mathbf{e}_i, t) + N_i^{\mathrm{BGK}}(\mathbf{x} - \mathbf{e}_i, t) \tag{3}$$

where

$$N_i^{\mathrm{BGK}}(\mathbf{x}, t) = \omega N_i^{\mathrm{eq}}(\mathbf{x}, t) - \omega N_i(\mathbf{x}, t) \tag{4}$$

$N_i^{\mathrm{eq}}(\mathbf{x}, t)$ are the equilibrium distributions and ω is the relaxation parameter which controls the viscosity of the fluid (Qian et al., 1992).

The solid or void nature of the node points imposes a length scale on each lattice point. When modelling geological media, the scale of a node is limited to the grain scale, which computationally restricts large-scale models. By modifying the BGK method with the introduction of a porous modification term ΔN^{PM}, given in Eq. (5), the length scale restriction can be overcome (Dardis and McCloskey, 1998a).

$$\Delta N_i^{\mathrm{PM}} = n_{\mathrm{s}}(\mathbf{x})[N_{i+3}(\mathbf{x}, t) - N_i(\mathbf{x} - \mathbf{e}_i, t)] \tag{5}$$

The addition of ΔN_i^{PM} into Eq. (3) allows the nodes to have a real numbered value in the interval [0,1] representing the solid density n_{s} which is $(1 - \phi)$ where ϕ is the connected porosity. Eq. (3) becomes:

$$N_i(\mathbf{x}, t + \Delta t) = N_i(\mathbf{x} - \mathbf{e}_i, t) + N_i^{\mathrm{BGK}}(\mathbf{x} - \mathbf{e}_i, t) + \Delta N_i^{\mathrm{PM}} \tag{6}$$

A node point is now no longer solid or void but has a value representing the connected porosity. The connected porosity can be considered to be an average value over any scale enabling a node to be defined on any scale. For low solid densities, the simulated permeability k has been shown to be consistent with the Kozeny–Carman equation relating k and ϕ, while for high solid densities there is a power law relationship between k and ϕ (Dardis and McCloskey, 1998b). Maillot and Main (1996) have also previously used a BGK scheme to model fluid flow in heterogeneous anisotropic media, including gravity.

Fluid flow in natural porous media is assumed to obey Darcy's law:

$$\mathbf{q} = -\frac{k}{\eta} \cdot \nabla \mathbf{p} \tag{7}$$

The law expresses the linear relationship between the volume averaged fluid velocity $\mathbf{q}$ and the volume averaged pressure gradient $\nabla\mathbf{p}$, where η is the dynamic viscosity. The modified BGK scheme obeys Darcy's law as seen from the example in Fig. 2. The porosity was assigned a fractal distribution with a Hurst exponent of 0.22 with a correlation length equal to the lattice size in the y-direction and effectively infinite in the x-direction. The porosity ranges from 0 to 7% (Fig. 2(A)). These figures are comparable to measured porosities (Oelkers, 1996) and fractal dimensions for sandstones (Korvin, 1992). Fluid was forced to flow-through the porous medium for several different pressure gradients in the direction shown in Fig. 2(A). The pressure gradient was implemented by applying a body force in the x-direction. A more detailed discussion of the boundary conditions and pressure gradients is

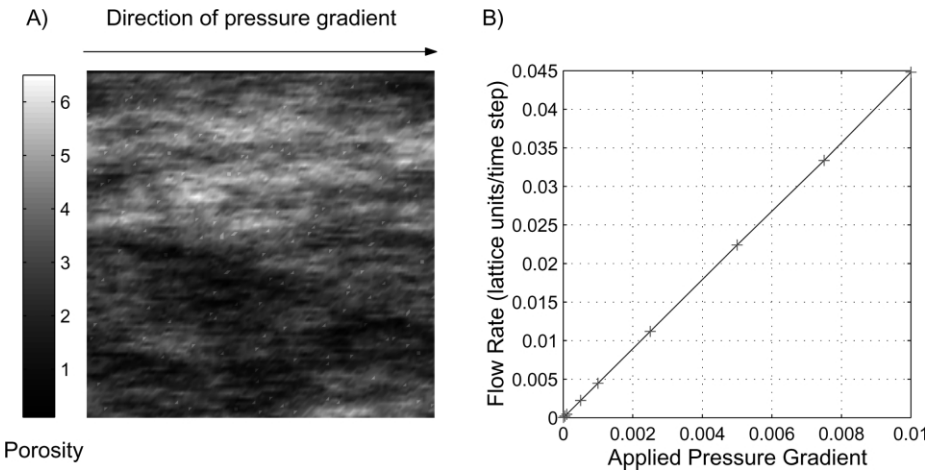

Fig. 2. The figure shows the fractal porosity field used in the simulation (A) and the flow rate versus the applied force (B). A Hurst exponent of 0.22 with a correlation length equal to the lattice size in the *y*-direction and effectively infinite in the *x*-direction was used. A straight line is plotted through the data points represented by +. The *x*-axis is the applied pressure gradient and the *y*-axis is the flow rate. When the grid is rescaled from numerical units to physical units the permeability from the slope of the line is 0.037 darcys.

given in Chen and Doolen (1998) and Kandhai et al. (1999). When the resultant flow rate versus the pressure gradient is plotted (Fig. 2(B)) a straight line can be fitted to the data confirming the flow rates predicted by the scheme are consistent with Darcy's law. Rescaling the numerical units to physical units for a grid of 100 m^2 gives a permeability of 0.037 darcys which is a reasonable permeability for a sandstone (Oelkers, 1996). This scheme was chosen because of its inherent parallelisability on multiple processors and the ease with which complex boundary conditions can be incorporated. The code was written in C and parallelised using MPI to run on a Beowulf cluster.

3. Passive transport

3.1. Transport model

In this section, the diffusion and advection of non-reactive species (conservative tracers) is discussed. The flow of fluids transports reactive species through a system, and therefore plays a fundamental role in controlling the rates and extents of reaction. To replicate accurately any geological reactive system, the model must incorporate transport in heterogeneous porous media. The diffusion and advection of a non-reactive species dissolved in a fluid is given by the hydrodynamical equation

$$D\cdot\nabla^2 C - \mathbf{v}\cdot\nabla C = \frac{\partial C}{\partial t} \tag{8}$$

where C is the concentration of the species, D is the diffusion coefficient and $\mathbf{v}$ is the velocity of the fluid. There have been several recent schemes using BGK methods to solve this equation (McNamara, 1990; Ponce Dawson et al., 1993; Flekkoy, 1993). Each scheme treats species in a manner similar to the actual lattice fluid, allowing them to reproduce accurately advection and diffusion effects in a fluid. In two dimensions, using a hexagonal grid, there is a requirement to store seven numbers per lattice site for each species using the BGK method. However, in realistic geological systems, the number of dissolved species in solution can be vast, and with large grids this can become very memory intensive and time consuming. For this reason, direct coupling of the species to the lattice fluid, as in the methods outlined above, could not be applied readily to large geological systems.

By contrast, in our scheme, species are introduced independently of the BGK method. They are transported through the system by a solution to Eq. (8)

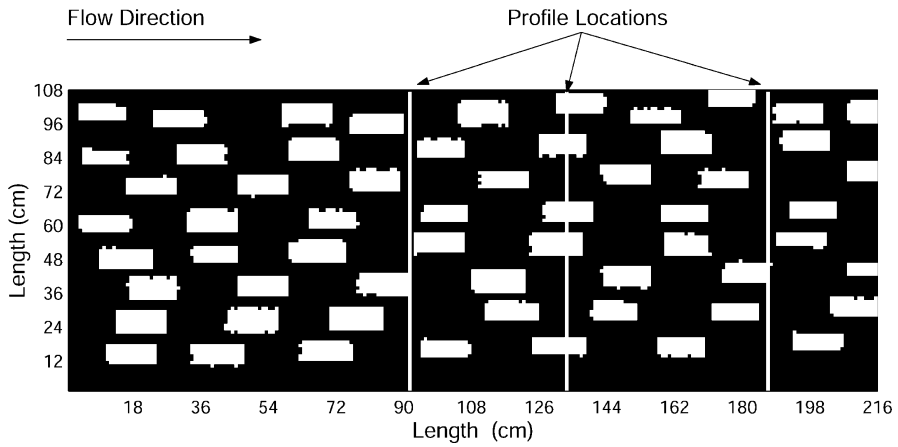

Fig. 3. The flow-cell from Silliman and Simpson (1987) with uniform heterogeneous packing used for our numerical simulation of their experiment. The white blocks are fine grain sand ($\phi = 0.38$) implaced in a coarse grain sand ($\phi = 0.405$). The profile locations indicate the position of the electrodes used to measure the breakthrough curves in the physical experiment.

using information from the BGK scheme given by:

$$C_i = \frac{C_0}{2}\mathrm{erfc}\left(\frac{\mathbf{x} - \mathbf{v}t}{2\sqrt{Dt}}\right) + \frac{C_0}{2}\exp\left(\frac{\mathbf{vx}}{D}\right) \mathrm{erfc}\left(\frac{\mathbf{x} + \mathbf{v}t}{2\sqrt{Dt}}\right) \quad (9)$$

where C_0 is the initial concentration. To solve the transport of a species using Eq. (9), given the initial concentration and the diffusion coefficient, the variables x, t and v must be determined. The velocity field $\mathbf{v}$ in a porous medium is determined at each node from the BGK technique. The concentration C_i transported to the nearest neighbour i can then be calculated by letting x be the internode spacing and t the time step from the BGK lattice. An upwind leap frog finite difference solution to the advection–diffusion equation coupled to the LB method could be a more useful alternative for passive transport and is being investigated.

3.2. Passive transport verification

The method outlined above was applied to the transport of a passive tracer in a porous medium. We compare our results to a physical experiment conducted by Silliman and Simpson (1987) to investigate the scale effect of dispersion of solutes using a laboratory flow-cell. The flow-cell ($2.4 \times 1.07 \times 0.01$ m^3) was packed with different arrangements of sand, and a passive tracer was injected as a step increase in concentration, which was measured at several intervals from the source. The specifics of the experimental set-up and results are given in Silliman and Simpson (1987) and Berkowitz et al. (2000). In testing the transport of species in a porous medium, we have considered only the case of uniform heterogeneity packing. This arrangement consists of blocks of fine-grained sand emplaced in a coarse grain sand (Fig. 3). The figure shows the location of three electrodes (profile locations) used to measure the concentration levels at intervals $L_1 = 0.91$ m, $L_2 = 1.37$ m and $L_3 = 1.87$ m from the inlet. The porosity of the coarse grain sand is 40.5%, while that of the fine grain blocks is 38%. This porosity value of the fine grain sand used in our numerical simulations was taken from Beard and Weyl (1973) for artificially mixed and wet packed sands for the quoted grain size in Silliman and Simpson (1987). The breakthrough curves at the three locations as calculated in our scheme are plotted against the laboratory experimental data and the Gaussian solution (Eq. (9)) using the experimental values in Fig. 4. The Gaussian solution is the solution using Eq. (9) and the experimental values for the flow rate and dispersion measured at that profile location. The Gaussian solution does not give a good fit to the experimental data. Our numerical results for the first two curves $L_1 = 0.91$ m and $L_2 = 1.37$ m agree well with the data and give a better fit than the Gaussian

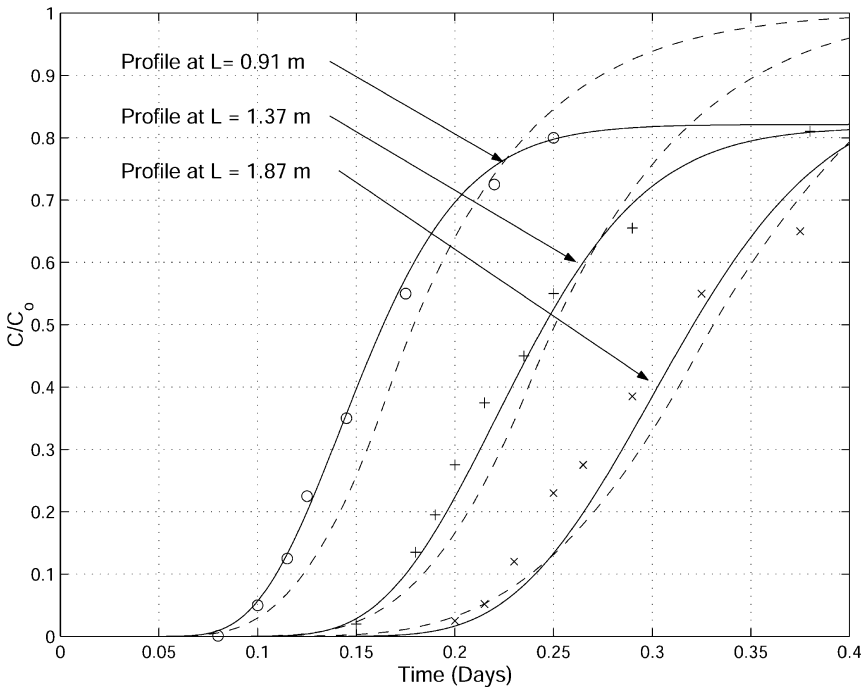

Fig. 4. The breakthrough curves are plotted for the three profiles. The solid lines indicate the numerical results while the symbols show the laboratory results for the different profile locations as shown in Fig. 3. The dashed line represents a Gaussian solution using the experimental values for the flow rate and dispersion at that profile location.

solution. The third curve $L_3 = 1.87$ m arrives at a time later than predicted from the laboratory data. This discrepancy can be explained by our inability to accurately replicate the correct velocity field as we cannot replicate the flow-cell packing in detail. In the physical experiment, the fluid velocity decreased from top to bottom, which is attributed to the non-uniformity in the packing of the flow-cell. The velocity was also not constant with distance through the cell. The experimental fluid velocities at the electrodes are quoted as $v_1 = 5.43$ m/day, $v_2 = 5.70$ m/day, and $v_3 = 5.79$ m/day. The experimental values of the dispersivity α, which is the ratio of the dispersion coefficient to the velocity, are quoted as $\alpha_1 = 0.073$ m, $\alpha_2 = 0.075$ m, and $\alpha_3 = 0.127$ m. These velocities and dispersivities were calculated from the breakthrough curves by Silliman and Simpson (1987) assuming Fickian diffusion and are considered to be approximate values only. Our numerical velocities are $v_1 = 5.59$ m/day, $v_2 = 5.72$ m/day, and $v_3 = 5.74$ m/day while our calculated dispersivities are $\alpha_1 = 0.077$ m, $\alpha_2 = 0.076$ m, and $\alpha_3 = 0.075$ m. The velocity and dispersivity in the numerical simulation at $L_3 = 1.87$ m are lower than the experimental values which could account for the late arrival of the tracer. The results presented above indicate that the scheme is capable of replicating advection and diffusion through heterogeneous media.

4. Reactive transport

4.1. Reactive transport model

With the introduction of reactive mineralogy, we can examine the changes in fluid flow related to porosity changes as a consequence of mineral dissolution/precipitation. This is achieved by allowing the chemical species to react with the porous medium. In our scheme, we consider only the primary species and their associated reactions. The effects of ion-exchange, absorption and desorption are not dealt with but can be easily included as a change in concentration levels. In geological media, species in

solution react with each other and with the rock minerals. The rates are governed by reaction kinetics and the maximum extent of reaction by equilibrium constants or solubility products for the specific species and minerals under consideration. Reactions between species in solution or between chemical species and minerals are governed by the species activity rather than their concentration. The activity a_i of a species i is the concentration multiplied by the activity coefficient to take account of electrostatic interactions between ions in solution. Activity coefficients are calculated using the Davies equation, which is an alternative form of the Debye–Huckel equation (Drever, 1997) and is applicable over a wider range of ionic strength. The equilibrium activities of species are calculated from equilibrium constants for each reaction involving that species. The equilibrium constants K_{eq} can be calculated from standard thermodynamic tables, using the Van't Hoff equation to account for the temperature dependence where appropriate (Drever, 1997). The Van't Hoff equation is valid between 0 and 100 °C. Outside this temperature range, temperature dependent laboratory derived equilibrium and reaction constants are used in all calculations. The rate of change of any reactive system is governed by the kinetics of the slowest reaction in that system. Generally, the rate at which geological species in solution equilibrate is higher than the rate of silicate mineral dissolution/precipitation. This permits the species in solution to be treated as if they reach equilibrium instantaneously, as the rate limiting process is the silicate mineral reaction rate. The rate limiting mechanisms of mineral dissolution can be controlled by three main processes, transport of solute to and away from the mineral surface, bond breaking or formation at the surface, or a combination of both. Most mineral reactions are controlled by bond breaking or formation (Berner, 1978). Mineral dissolution/precipitation can be expressed by the general rate equation in mol/s (Aagaard and Helgeson, 1982; Lasaga, 1984).

$$\text{Rate} = \frac{\text{Surface area}}{\text{Volume}} \nu k_+ (a_{H^+})^n - \frac{\text{Surface area}}{\text{Volume}} \times \nu \frac{Q}{K_{eq}} k_+ (a_{H^+})^n \quad (10)$$

where ν is the stoichiometric number, Q is the activity quotient, k_+ is the forward rate constant and K_{eq} is the solubility of the mineral and n is a real number in the interval 0–1. The values of K_{eq} and k_+ can be found from temperature and pH dependent functions from laboratory experiments. The rate is also dependent on the surface area to volume ratio. This ratio can be inferred from geometrical considerations or from measurements using gas adsorption techniques, BET techniques (Brunauer et al., 1938). Thus, Rimstidt and Barnes (1980) quote area to volume ratios for several geometries, including spherical grains, fractures or cylindrical pipes. When considering these simple geometries, the effect of surface roughness, defined as the ratio of real reactive surface area to the geometric surface area of a smooth surface encompassing the actual surface, should be taken into account. Surface roughness values for minerals can extend to over three orders of magnitude. Anbeek (1992) quotes surface roughness values for naturally weathered feldspar surfaces in the range 130–2600 while for freshly created surfaces, roughness factors ranged from 2.5 to 11. Channelling of reactive flow is common in natural systems and this typically can lower the reactive surface value by several orders of magnitude. When inputting reactive surface areas into models, the specifics of the mineralogy and the flow patterns in the system under investigation should be considered. This is essential to take account of the effect of surface roughness and channelling to give a realistic estimate of the rate of mineral dissolution/precipitation.

4.2. Reactive transport verification

To verify the reactive transport, we have simulated two independent flow-through experiments from the literature focusing on quartz. Quartz was chosen as it is an abundant mineral in the Earth's crust and the reaction rate and solubility of quartz is relatively well documented. The quartz–water system is governed by the equation:

$$2H_2O + SiO_2 \Leftrightarrow H_4SiO_4 \quad (11)$$

In simulating the quartz dissolution experiment, the forward rate constant k_+ is from Rimstidt and Barnes (1980) and the solubility constant of quartz K_{eq} is from Rimstidt (1997). Both values are functions of temperature and are valid in the range 0–300 °C. There are several quoted rate constants for quartz

Table 1
Parameters used in the flow-through experiments. These values remained fixed through our numerical simulations of the laboratory dissolution experiments

Parameters	Kieffer et al.	Johnson et al.
Temperature (°C)	80	239
BET surface area (m^2/g)	0.06	0.05
Flow rate (m/yr)	542.2	622.1
PH	10.4	7
Porosity (%)	5.1	42.5

dissolution (Oelkers, 1996), and we have used Rimstidt and Barnes (1980) as it is an intermediate value. The solubility of quartz is approximately constant at a range of low pH values. Above a pH of 8.5, H_4SiO_4 dissociates readily, increasing the solubility. The solubility constant of quartz then becomes dependent on the dissociation constants of H_4SiO_4 (Stumm and Morgan, 1981). The quartz constants were chosen as they are relevant to the problem but are also independent of the flow-through experiments we chose to model. For all the simulations, we have used the quoted BET surface areas of the relevant physical experiment, which were kept constant throughout the simulations.

We have simulated the experiments of Kieffer et al. (1999) and Johnson et al. (1998). We are interested only in the parameters used to conduct the experiments and so specific details on the methodology used can be found in the papers referred to above. The effluent Si concentration values observed in the laboratory experiments are considerably lower than the equilibrium concentrations. This indicates the outlet Si concentrations observed are steady state values and not equilibrium concentrations. The parameters used in the dissolution experiments taken from Johnson et al. (1998) and Kieffer et al. (1999), listed in Table 1, were used as inputs for our model. Kieffer et al. (1999) carried out a flow-through experiment at 80 °C on a clean sandstone to investigate the relationship between the reactive surface area and porosity, permeability and fluid flow rate. The comparison of the laboratory results

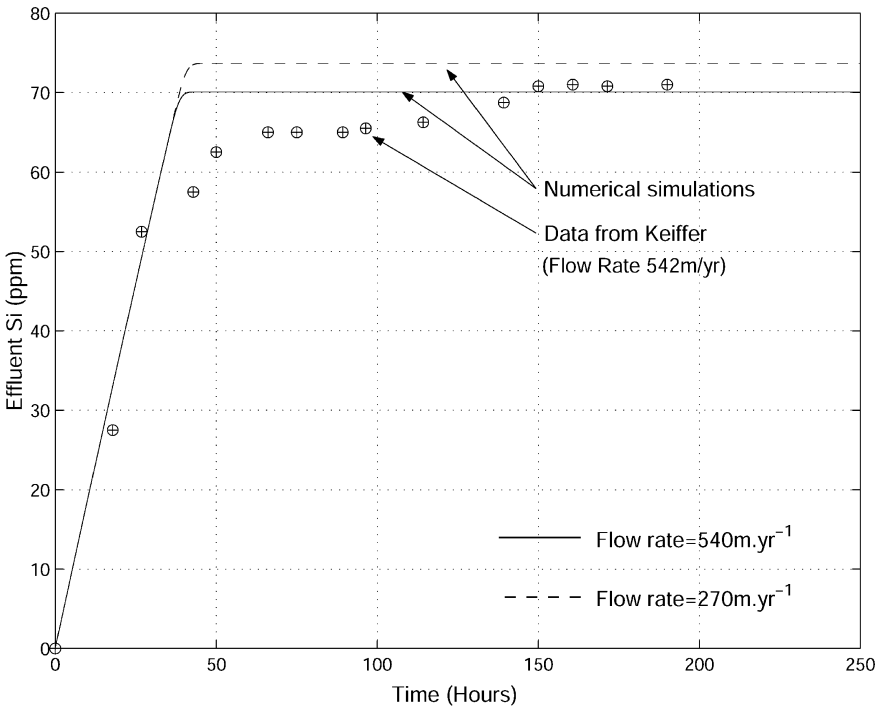

Fig. 5. The figure shows the comparison between the data from Kieffer et al. (1999) (circles) and the modelled results (solid and dashed lines). The steady state values from Kieffer et al. (1999) are 70.8 ppm for a flow rate of 542.2 m/yr and 74.1 ppm for 271.1 m/yr. Both results agree well with our simulation (70.1 and 73.7 ppm). No error bars on the effluent Si were quoted for the experimental data.

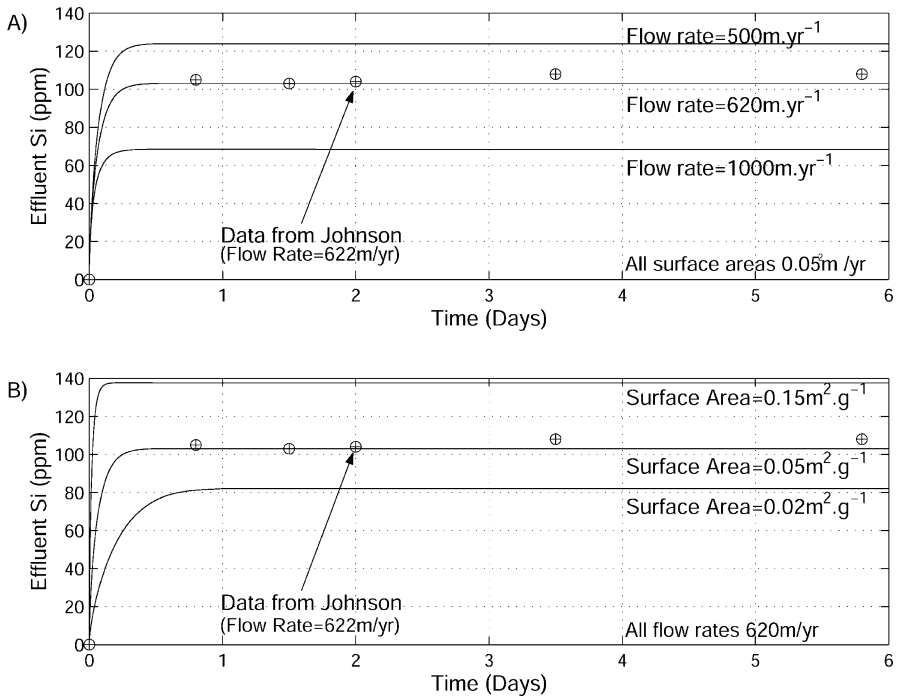

Fig. 6. The figure shows the comparison between the data from Johnson et al. (1998) (circles) and the modelled results (lines). The flow rate was varied in (A) and the surface area was varied in (B) to examine the sensitivity of the code. The higher the flow rate the lower the residence time of the fluid hence there is less [Si]. The more surface area, the more mineral is available to react hence an increase in [Si] output with a higher surface area. The parameters used by Johnson et al. (1998) are for a flow rate of 622 m/yr and a surface area of 0.05 m^2/g. No error bars on the effluent Si were quoted for the experimental data.

with the output from our model are shown in Fig. 5. The steady state effluent Si concentration is quoted as 70.8 ppm while our steady state value is 70.1 ppm for the values listed in Table 1. Halving the flow rate from 542.2 to 271.1 m/yr in the laboratory experiment gave a steady state value of 74.1 ppm. Our simulated value for this flow rate is 73.7 ppm. Both steady state values from our numerical simulation agree well with the experimental data. However, the transition from the advection phase to the steady state phase (non-linear part of the curve) is much narrower in the model than it is for the laboratory data. Given the associated errors with the experiment and measuring BET surface areas ($\pm 14\%$) along with the use of a homogeneous lattice in the numerical simulations may account for this discrepancy.

Johnson et al. (1998) used a plug-flow reactor experiment on quartz to experimentally determine steady state effluent concentrations. Using the experimental values (Table 1) we have reproduced the correct effluent concentration (Fig. 6(A)). We have also varied the flow rate and surface areas to check the sensitivity of our model. Fig. 6(A) shows the effluent concentration through time for different flow rates and Fig. 6(B) shows the effluent concentration through time for different surface areas. The flow rate controls the residence time of the fluid in the system with higher residence times (lower flow rates) resulting in higher steady state Si values. By lowering the surface area the fluid reacts with less mineral, hence the steady state values decrease. In both cases, the results are consistent with the expected behaviour.

One of the major numerical and experimental observations is that the steady state concentrations are recovered after less than 1 day, even at these relatively low temperatures for a quartz system. At lower temperatures (20 °C) similar rapid transitions are obtained for a feldspar dissolution process after 150 h (fig. 12(a) of Main et al. (1994)). In that paper the dissolution was also associated with detectable

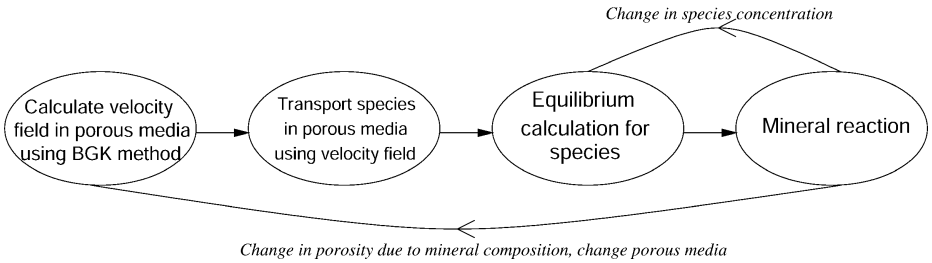

Fig. 7. The figure shows a schematic of the method used to model reactive fluid flow in porous media.

changes in the permeability, implying a positive feedback mechanism between flow, dissolution and enhanced flow. In the model presented this would involve feedback to the local connected porosity, probably leading to local flow channelling. The major conclusion from observing fluid chemistry changes during flow experiments is that, although steady state concentrations are very low, here hundreds of parts per million, the reaction rates are relatively rapid compared to geological timescales. This was not obvious before accurate liquid chromatography became available, because it can be hard to see evidence of dissolution textures on a laboratory timescale since the amount of material involved is minimal. Of course this is not the case on geological timescales. In summary, we have outlined a scheme for modelling reactive fluid flow in porous media using the BGK method. The species are allowed to react with the porous media governed by experimentally determined reaction rates and equilibrium constants. Changes in the porosity of the media due to geochemical reactions are then fed back into the BGK method and the new velocity field is calculated in the new porosity field. A schematic representation of the reactive flow model showing the major feedbacks is given in Fig. 7.

5. Alteration of quartz–feldspar rock

In the previous sections, we have discussed our scheme in relation to laboratory scale experiments conducted over short time periods. Geological models need to be valid over long time periods and large volumes. Two numerical examples of the alteration of a rock through a 100 m profile over a period of 30,000 years is presented in this section. The system under examination is a quartzofeldspathic lithology. We have chosen these minerals as they, along with calcite, represent the most abundant minerals in the Earth's crust. The first example consists of a host rock comprised of 60% quartz, 10% albite and the remaining an inert mineral. In the second example, we replace the albite with K-feldspar. The rock is assigned a homogeneous porosity of 10% at a constant temperature of 130 °C with the fluid flowing at 2 m/yr and with a diffusion coefficient of 0.05 m^2/yr. The parameters used are possible values for the flow rate and composition of a sandstone aquifer. The diffusion coefficient chosen is characteristic of many aqueous species (Oelkers, 1996). At time zero water in equilibrium with quartz at a pH of 4 enters the rock. We have not included any heterogeneity in the system as the example is used to illustrate that the scheme produces results, which are geologically reasonable. Feldspar reacts with water to produce clay minerals. The stability of the clay minerals depends on the particular geochemical environment. For the albite–quartz case, the formation of a particular clay mineral and its stability is dependent on the H_4SiO_4 activity and the $[Na^+]/[H^+]$ ratio in the groundwater. In the K-feldspar case $[Na^+]/[H^+]$ ratio is replaced by the $[K^+]/[H^+]$ ratio. The reaction of feldspar will change the groundwater composition, which could in turn cause the initially produced clay mineral to become unstable. This leads to an alteration sequence as one clay mineral converts to a more stable mineral. The stability of the clay minerals was determined using standard thermodynamic data. The alteration sequence is shown in Fig. 8 for three different time periods. The sequence of alteration is from albite to gibbsite to kaolinite. In the second example, the albite is replaced with K-feldspar at a lower temperature of 25 °C. All the other parameters remain the same. The

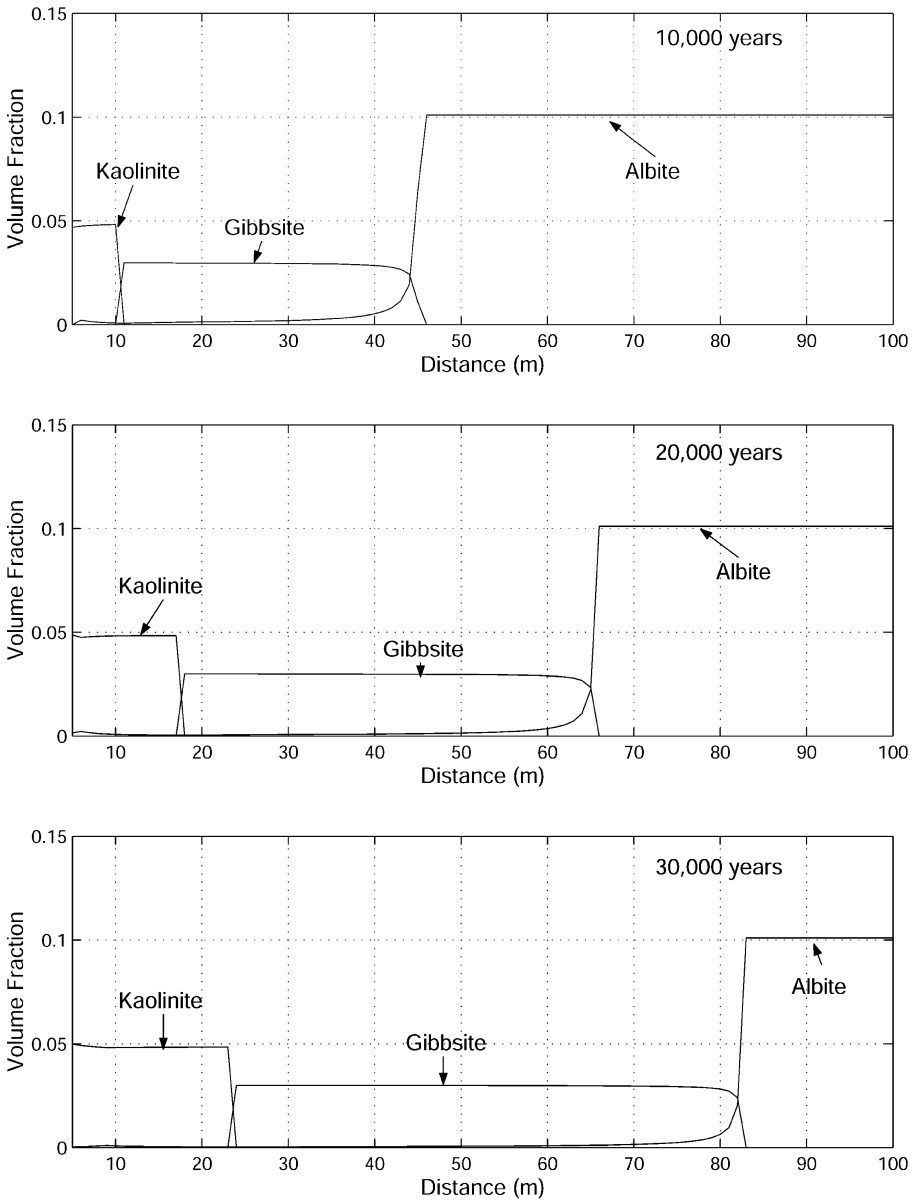

Fig. 8. The alteration of a quartz–albite rock as water at 130 °C penetrates from the left. Albite alters to gibbsite, which in turn is replaced by kaolinite. The flow direction is from left to right.

alteration sequence is from K-feldspar to muscovite to kaolinite and is shown in Fig. 9. In both cases, the kaolinite grows continuously with time while the gibbsite zone (Fig. 8), and the muscovite zone (Fig. 9), propagates in the flow direction. For the lower temperature in the second example, the rate of dissolution of K-feldspar is approximately three orders of magnitude lower than that of albite in the first example. This slow reaction rate does not enable the complete dissolution of K-feldspar in the time periods under consideration. The dissolution of the feldspar and the creation of the clay minerals can lead to three different changes in porosity. There can be intergranular replacement where the clay minerals

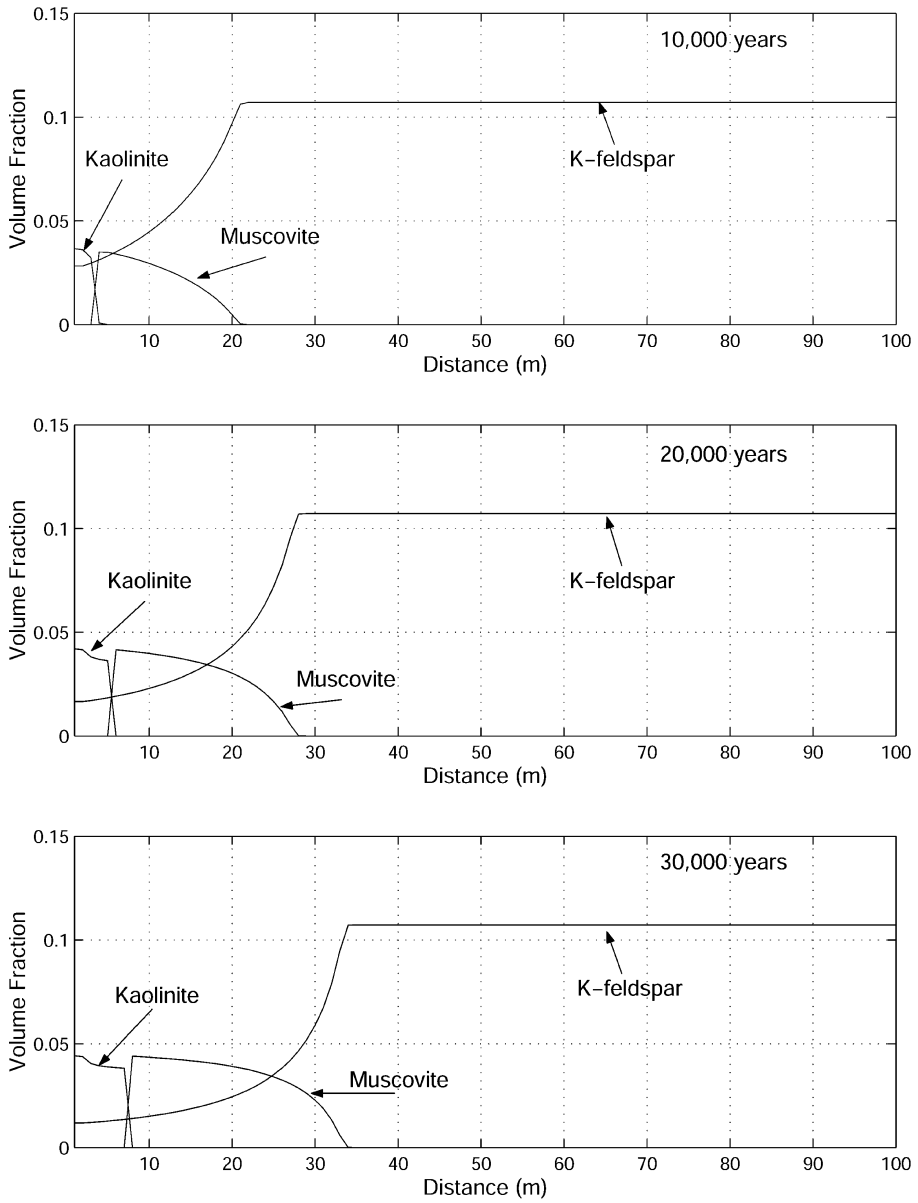

Fig. 9. The alteration of a quartz–K-feldspar rock as water penetrates from the left. The K-feldspar alters to muscovite, which in turn is replaced by kaolinite. At 25 °C insufficient time has elapsed for extensive replacement of K-feldspar. The flow direction is from left to right.

replace the feldspar within the grains leading to an increase in porosity. The clay minerals, which replace the feldspar, can be completely transported out of the system giving a larger increase in porosity than the previous case. Finally, the clay minerals may be transported through the system, but cause blocking of pores and a decrease in the connected porosity. Considering the first case, the dissolution of the feldspar and the creation of the clay minerals lead to a decrease in rock volume. This will increase the porosity and hence the flow rate due to an increase in void space. The change in porosity and flow rate after 30,000 years for both examples are shown in Fig. 10. However, in reality compaction may decrease the

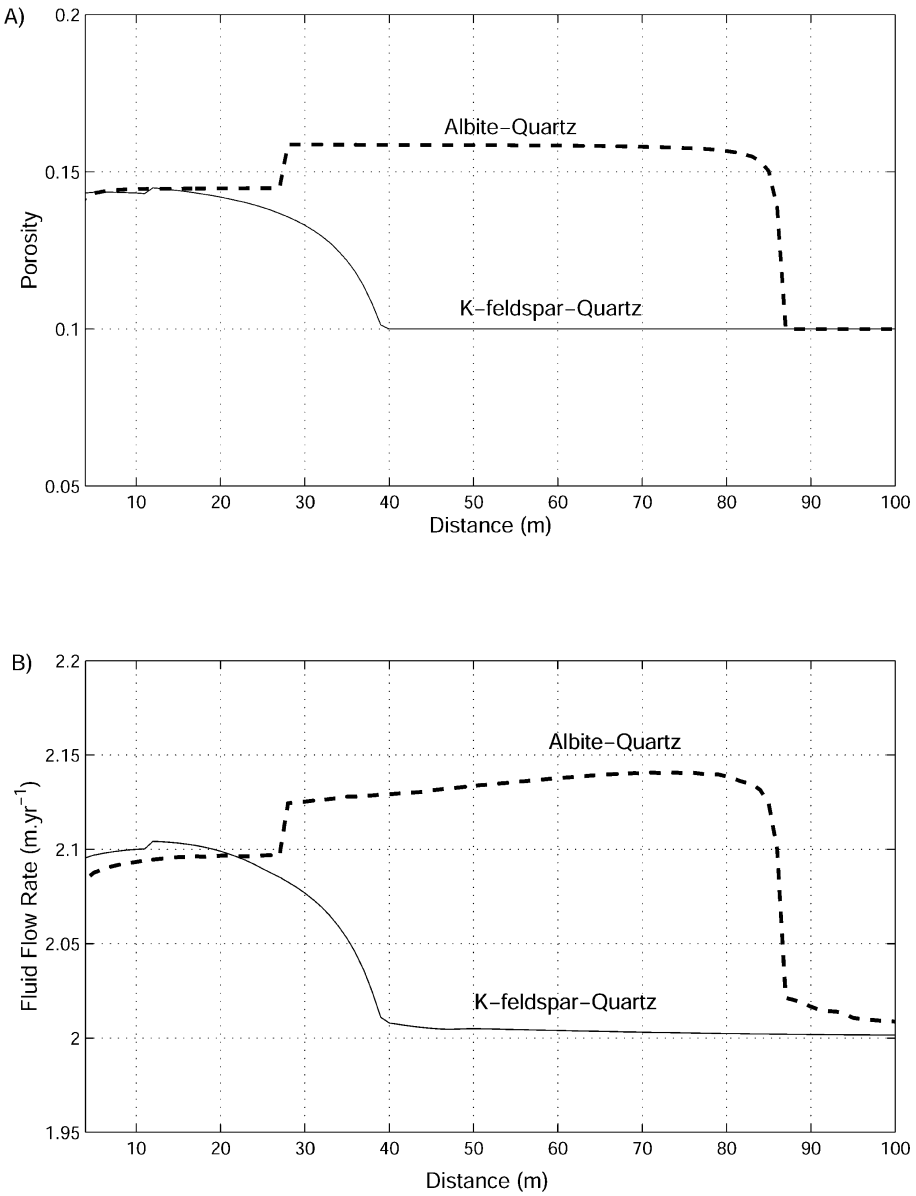

Fig. 10. The alteration of a quartz–feldspar host rock as water penetrates from the left leads to a loss in rock volume. The resultant change in porosity after 30,000 years is shown in (A). (B) shows the change in flow rate through the host rock as a result of the increase in porosity. The dashed line represents the albite–quartz example while the solid line represents the K-feldspar–quartz example. The flow direction is from left to right.

porosity and the clay minerals produced tend to block up the pores decreasing the permeability. These effects were not considered in this simple case. The results presented for both cases can be considered to be geologically reasonable even though the example presented is over simplified. Lichtner (1996) presents some numerical work on the alteration of quartz–feldspar rocks to illustrate the formation of ghost zones. Our results including the feedback between the geochemical reactions and the porosity are qualitatively consistent with results from Lichtner's scheme.

6. Summary

We have outlined a numerical scheme for the transport of reactive species through porous media. The scheme has not just been tested, it has been validated against laboratory experiments for both passive and reactive transport. The results from the numerical scheme are consistent with experimental data. Applying the model to a geologically realistic rock over long time periods gives results which are consistent with other numerical work and which are geologically plausible. The scheme is ideally suited for parallel computing and can be easily extended to three dimensions. The incorporation of heterogeneity in the model can enable the modelling of geological media where fractal statistics in fracture networks and permeability play an important role in controlling fluid flow. The method outlined is general enough to allow investigations of a range of geological processes where the effects of changing flow regimes as a consequence of porosity reduction or increase from mineral dissolution/precipitation play an important part in our understanding of these processes. The current scheme is for an incompressible fluid and only small variations in density can be modelled. This restricts the inclusion of large pressure differences into our model. Recently, lattice BGK schemes, have been developed to simulate compressible flows, including temperature driven flows (Vahala et al., 1998; Yu and Zhao, 2000). These developments can be incorporated in our scheme to overcome the pressure and temperature limitations. The introduction of stress into the scheme would enable the modelling of pressure-solution deformation of rocks, which is the dominant mechanism of ductile deformation in the upper part of the crust. We are currently investigating a method for incorporating a stress field. We intend to apply our scheme to several areas where reactive flow and heterogeneity influences the evolution of the system, including fault sealing and environmental groundwater flow. We also intend to extend the scheme to three dimensions and to update the geochemical database to include a wider range of mineral phases.

Acknowledgments

The authors wish to thank Ian Main and Bertrand Maillot for their useful comments and suggestions which greatly improved the original manuscript.

References

Aagaard, P., Helgeson, H., 1982. Thermodynamics and kinetic constraints on reaction rates among minerals. Am. J. Sci. 282, 237–285.

Anbeek, C., 1992. Surface roughness of minerals and implications for dissolution studies. Geochim. Cosmo. Acta 56, 1461–1469.

Beard, D.C., Weyl, P.K., 1973. Influence of texture on porosity and permeability of unconsolidated sand. AAPG Bull. 57, 349–369.

Berkowitz, B., Scher, H., Silliman, S.E., 2000. Anomalous transport in laboratory-scale, heterogenous porous media. Water Resour. Res. 36 (1), 149–158.

Berner, R.A., 1978. Rate control of mineral dissolution under earth surface conditions. Am. J. Sci. 278, 1235–1252.

Bolton, E.W., Lasaga, A.C., Rye, D.M., 1997. Dissolution and precipitation via forced-flux injection in a porous medium with spatially variable permeability. J. Geophys. Res. 102 (B6), 12, 159–12,171.

Bolton, E.W., Lasaga, A.C., Rye, D.M., 1999. Long-term flow/chemistry feedback in a porous medium with heterogeneous permeability. Am. J. Sci. 299, 1–68.

Bonnet, E., Bour, O., Odling, N.E., Davy, P., Main, I., Cowie, P., Berkowitz, B., 2001. Scaling of fracture systems in geological media. Rev. Geophys. 39, 347–383.

Brunauer, S., Emmett, P.H., Tallant, E., 1938. Adsorption of gases in multimolecular layers. J. Am. Chem. Soc. 60, 309–319.

Canals, M., Meunier, J.D., 1995. A model for porosity reduction in quartzite reservoirs by quartz cementation. Geochim. Cosmo. Acta 59 (4), 699–709.

Chen, S., Doolen, G.D., 1998. Lattice Boltzmann methods for fluid flow. Annu. Rev. Fluid Mech. 30, 329–364.

Dardis, O., McCloskey, J., 1998a. Lattice Boltzmann with real numbered solid density for the simulation of flow in porous media. Phys. Rev. E 57, 4834–4837.

Dardis, O., McCloskey, J., 1998b. Permeability porosity relationships from numerical simulations of fluid flop. Geophys. Res. Lett. 25 (9), 1471–1474.

Drever, J.I., 1997. The Geochemistry of Natural Waters, Prentice-Hall, Englewood Cliffs, NJ.

Flekkoy, E., 1993. Lattic BGK models for miscible fluids. Phys. Rev. E 47 (6), 4247–4257.

Frisch, U., Hasslacher, B., Pomeau, Y., 1986. Lattice-gas automata for the Navier–Stokes equation. Phys. Rev. Lett. 58, 1505–1508.

Johnson, J.W., Knauss, K.G., Glassley, W.E., DeLoach, L.D., Tompson, A.F.B., 1998. Reactive transport modelling of plug-flow reactor experiments. J. Hydrol. 209, 81–111.

Kandhai, D., Koponen, A., Kataja, M., Timonen, J., Sloot, P.M.A.,

1999. Implementation aspects of 3D lattice-BGK: boundaries, accuracy, and a new fast relaxation method. J. Comput. Phys. 150, 482–501.

Kieffer, B., Jove, C., Oelkers, E., Schott, J., 1999. An experimental study of the reactive surface area of the Fontainebleau sandstone. Geochim. Cosmo. Acta 63 (21), 3525–3534.

Korvin, G., 1992. Fractal Models in the Earth Sciences, Elsevier, Amsterdam.

Lasaga, A.C., 1984. Chemical kinetics of water–rock interactions. J. Geophys. Res. 89 (B6), 4009–4025.

Lichtner, P.C., 1996. Continuum formulation of multicomponent–multiphase reactive transport. Rev. Mineral. 34, 1–79.

Lichtner, P.C., Steefel, C.I., Oelkers, E.H., 1996. Reactive transport in porous media. Rev. Mineral., 34.

Maillot, B., Main, I.G., 1996. A lattice BGK model for the diffusion of pore pressure, including anisotropy, heterogeneity and gravity effects. Geophys. Res. Lett. 23, 13–16.

Main, I.G., Smart, B.G.D., Shimmield, G.B., Elphick, S.C., Crawford, B.R., Ngwenya, B.T., 1994. The effects of combined changes in pore-fluid chemistry and stress state on permeability in reservoir rocks: preliminary results from analogue materials. In: Aasen, O., (Ed.), North Sea Oil and Gas Reservoirs, vol. III. Kluwer, Dordrecht, pp. 357–370.

McNamara, G., 1990. Diffusion in a lattice gas. Europhys. Lett. 12 (4), 329–334.

McNamara, G., Zanetti, G., 1988. Use of the lattice Boltzmann equation to simulate lattice-gas automata. Phys. Rev. Lett. 61, 2332–2335.

Oelkers, E.H., 1996. Physical and chemical properties of rocks and fluids for chemical mass transport calculations. Rev. Mineral. 34, 131–191.

Phillips, O.M., 1991. Flow and Reactions in Permeable Rocks, Cambridge University Press, New York.

Ponce Dawson, S., Chen, S., Doolen, G.D., 1993. Lattice Boltzmann computations for reaction–diffusion equations. J. Chem. Phys. 98 (2), 1514–1523.

Qian, Y., D'Humieres, D., Lallemand, P., 1992. Lattice BGK models for the Navier–Stokes equation. Europhys. Lett. 17, 479–484.

Rimstidt, J.D., 1997. Quartz solubility at low temperatures. Geochim. Cosmo. Acta 61 (13), 2553–2558.

Rimstidt, J.D., Barnes, H.L., 1980. The kinetics of silica–water reactions. Geochim. Cosmo. Acta 44, 1683–1699.

Silliman, S.E., Simpson, E.S., 1987. Laboratory evidence of the scale effect in dispersion of solutes in porous media. Water Resour. Res. 23 (9), 667–673.

Stumm, W., Morgan, J.J., 1981. Aquatic Chemistry, Wiley, New York.

Vahala, G., Pavlo, P., Vahala, L., Martys, N.S., 1998. Thermal lattice-Boltzmann models for compressible flops. Int. J. Modern Phys. C 9 (8), 1247–1261.

Yu, H., Zhao, K., 2000. Lattice Boltzmann method for compressible flows with high Mach numbers. Phys. Rev. E 61 (4), 3867–3870.